AGU PUBLICATIONS

JGR

Journal of Geophysical Research: Solid Earth

RESEARCH ARTICLE
10.1002/2016JB013180

Key Points:
- Spectral and multiplet analyses of precursory seismicity of the July 2008 vulcanian explosion
- Changes in rates and spectral content of waveforms highlight precursory changes in magmatic system
- Hybrid and LP events are part of the same source process, hence not separate event classifications

Correspondence to:
M. Rodgers,
mel.rodgers@earth.ox.ac.uk

Citation:
Rodgers, M., P. J. Smith, T. A. Mather, and D. M. Pyle (2016), Quiescent-explosive transitions during dome-forming volcanic eruptions: Using seismicity to probe the volcanic processes leading to the 29 July 2008 vulcanian explosion of Soufrière Hills Volcano, Montserrat, *J. Geophys. Res. Solid Earth*, *121*, 8453–8471, doi:10.1002/2016JB013180.

Received 16 MAY 2016
Accepted 23 OCT 2016
Accepted article online 26 OCT 2016
Published online 14 DEC 2016

Quiescent-explosive transitions during dome-forming volcanic eruptions: Using seismicity to probe the volcanic processes leading to the 29 July 2008 vulcanian explosion of Soufrière Hills Volcano, Montserrat

Mel Rodgers[1], Patrick J. Smith[2,3], Tamsin A. Mather[1], and David M. Pyle[1]

[1]Department of Earth Sciences, University of Oxford, Oxford, UK, [2]Montserrat Volcano Observatory, Flemmings, Montserrat, [3]Seismic Research Centre, University of the West Indies, Saint Augustine, Trinidad and Tobago

Abstract The July 2008 vulcanian explosion at Soufrière Hills Volcano (SHV), Montserrat, was preceded by one of the largest seismic swarms observed since the start of the eruption. We analyze the spectral and waveform properties of the earthquakes in this swarm and compare these observations to models of subsurface volcanic processes. We observe an initial volcano-tectonic (VT) swarm, followed by a large low-frequency (LF) swarm. We observe that the spectral content of LF events changes over time to carry more energy at lower frequencies. This shift to a lower frequency spectral content is concurrent with an increase in LF event rates. Ash-venting occurred a few hours before peak event rate. There was a subsequent increase in the higher-frequency energy component of LF events, concurrent with a decrease in event rates. Seismic quiescence occurred in the final 7 h before the vulcanian explosion. Our observations of VT seismicity are consistent with a model of decoupled gas ascent prior to magma emplacement. Changes in spectral properties and event rates suggest changes in conduit properties and/or pressure changes during magma ascent and stalling in the few days before the explosion. This interpretation is supported by previous petrological observations. Our analysis of repeating earthquakes suggests that hybrid and long-period events are part of the same source process and should not be considered separate classifications, at least at SHV. Our analysis highlights the potential of using simple spectral and waveform analyses for understanding changes in the magmatic system during transitions between quiescence and eruption.

1. Introduction

Vulcanian explosions are short-lived explosive eruptions that typically occur at andesitic to dacitic volcanoes [*Self et al.*, 1979; *Watt et al.*, 2007; *Clarke et al.*, 2015]. These violent episodes of explosive activity are often associated with long-lived dome-forming eruptions. Recent examples include Colima, Mexico; Santiaguito, Guatemala; Merapi, Indonesia; and Soufrière Hills Volcano, Montserrat [*Cassidy et al.*, 2015; *Bluth and Rose*, 2004; *Surono et al.*, 2012; *Cole et al.*, 2014a] and are often ascribed to the buildup of gas pressure within a cooling and crystallizing viscous magma in a shallow conduit [e.g., *Self et al.*, 1979; *Stix et al.*, 1997; *Diller et al.*, 2006], perhaps linked to changes in the flux of hotter magma at depth [e.g., *Preece et al.*, 2016].

During long-lived dome-forming eruptions volcanoes often go through transitions between quiescent, effusive, and explosive behavior. The rapid transition to explosive activity during dome-forming eruptions poses a significant challenge in terms of our capacity to detect and diagnose the change before it happens, and as a result, presents a significant risk [*Buurman et al.*, 2013; *Loughlin et al.*, 2002; *Lachowycz et al.*, 2013; *Ogburn et al.*, 2015]. Explosive phases are often associated with dome collapse events during dome growth and with effusive-explosive transitions [*Surono et al.*, 2012; *Druitt et al.*, 2002; *Edmonds and Herd*, 2007]. However, quiescent-explosive transitions can occur without associated dome growth or effusion, and these present a different challenge in terms of monitoring and risk perception [*Stix et al.*, 1997; *Major and Lara*, 2013]. Precursory behavior for such quiescent-explosive transitions can include seismic swarms, monochromatic low-frequency (LF) events, sustained tremor, ground deformation, increased ground temperature, and changes in monitored gas parameters [*Surono et al.*, 2012; *West*, 2013; *Stix et al.*, 1997], but they can also occur with few or minor precursory signals [*Major and Lara*, 2013].

1.1. Seismicity During Dome-Forming Eruptions

There have been many studies of LF seismicity accompanying dome-forming eruptions and vulcanian explosions. LF seismicity is a common feature to most, if not all, dome-forming eruptions and has been linked to pressurization of fluid-filled cracks [*Chouet et al.*, 1994; *Chouet*, 1996], degassing processes in a pressurized magma conduit/dome [*Stix et al.*, 1997; *Varley et al.*, 2010], and to the ascent of magma in a conduit [*Neuberg et al.*, 2006; *Hammer and Neuberg*, 2009]. Periods of seismic unrest do not always lead to eruption [*Moran et al.*, 2011; *Rodgers et al.*, 2015b]. However, the onset of LF events, or the appearance of LF swarms, is often interpreted as a short-term (hours-days-weeks) indication of eruption; thus, detection of LF seismicity is crucial to many aspects of volcano monitoring [*McNutt*, 1996; *Sparks*, 2003].

On Montserrat, where the Soufrière Hills Volcano (SHV) has been erupting for over 20 years, the Montserrat Volcano Observatory (MVO) classifies LF events as either long-period (LP) or hybrid events. Due to their high-frequency impulsive onset and low-frequency coda, hybrid events have been interpreted as brittle failure triggering resonance in a fluid-filled crack [*Lahr et al.*, 1994; *Neuberg et al.*, 2006]. However, an earthquake may appear as an LP on one station and as a hybrid on another (G. Thompson, personal communication 2015), perhaps due to rapid attenuation of high-frequency components of the waveform in certain source-receiver paths [*Harrington and Brodsky*, 2007]. At SHV the frequency-distribution analysis of earthquakes with energy below 2 Hz does not show the expected bi-modal distribution leading *Neuberg et al.* [2000] to suggest that these two event types represent end members of a continuum.

Spectral analysis is an important aspect of seismic analysis and monitoring at volcanoes. Spectrograms of continuous tremor signals show changing frequency content during dome-forming eruptions: *Neuberg and O'Gorman* [2002] identified upward gliding spectral lines in tremor during the December 1997 eruption of SHV, and *Hotovec et al.* [2013] identified strong upward gliding spectral lines in tremor during the 2009 eruption of Redoubt, Alaska. Detecting spectral changes within discrete earthquake swarms can reveal patterns of behavior during eruptions; for example, *Buurman and West* [2010] show lower frequency content before explosions during the 2006 eruption of Augustine. *Ketner and Power* [2013] observe a decrease in frequency content of waveforms in the precursory swarms of magmatic explosions during the 2009 eruption of Redoubt.

Repeating earthquakes are found during most significant seismic swarms at volcanoes [*West*, 2013], and their presence alone is not indicative of eruptive processes. Repeating LF waveforms have been observed in many different types of volcanic settings, including dome-forming eruptions at Redoubt, Alaska; Unzen, Japan; Mount St Helens, Washington; Bezymianny, Kamchatka; and SHV [*Power et al.*, 2013; *Lamb et al.*, 2015; *Thelen et al.*, 2011; *West*, 2013; *Green and Neuberg*, 2006; *Ottemöller*, 2008; *De Angelis*, 2009]; at persistently restless volcanoes such as Telica, Nicaragua, and Shishaldin, Alaska [*Rodgers et al.*, 2013, 2015a; *Petersen*, 2007]; and at basaltic systems such as Kilauea, Hawaii [*Battaglia et al.*, 2003]. Repeating families (multiplets) are often used to improve locations [*Battaglia et al.*, 2003], determine depth of explosive activity [*West*, 2013; *Thelen et al.*, 2011], constrain source mechanisms [*Green and Neuberg*, 2006], and assess the stability of seismic sources [*Rodgers et al.*, 2013] and the stability of stress fields [*West*, 2013].

1.2. The Ongoing SHV Eruption

SHV (Figure 1) began erupting in 1995, and for the last 20 years has repeatedly transitioned between quiescent, effusive, and explosive phases of activity (Figure 2) [*Kokelaar*, 2002; *Wadge et al.*, 2014]. Significant eruptions and seismic activity have occurred during that time, with many of the largest explosions occurring during dome growth or as major dome collapse events that marked the end of extrusion phases. For example, seismic activity preceded dome collapse events in 1997, including the Boxing Day dome collapse and lateral blast, and the July 2003 dome collapse event was associated with an intense seismic swarm; both of these marked the end of extrusive phases [*Kokelaar*, 2002; *Wadge et al.*, 2014]. On 29 July 2008 a vulcanian explosion marked the end of a quiescent phase (*Pause 3*) and the onset of an extrusive phase (*Phase 4*). The explosion that marked this sudden quiescence-explosion transition was one of the largest explosions by volume [*Cole et al.*, 2014a] and the largest to occur outside a period of lava extrusion and dome growth [*Cole et al.*, 2014a]. It was preceded by one of the most intense seismic swarms ever recorded at SHV, with rates of up to one event per minute at the height of the swarm (Figure 3). Previous work on multiplets from this intense seismic swarm focussed on using a subset of earthquakes to constrain changes in source displacement [*De Angelis*, 2009].

Figure 1. Inset bottom left: Location of Lesser Antilles volcanic arc. Inset top left: Location of Montserrat. Main: Location Map of Soufrière Hills Volcano, Montserrat, and seismic stations operational during the study period (the black triangles indicate broadband, and the blue triangles indicate short period). Montserrat Volcano Observatory is highlighted in red and marked as "MVO." Location of Gages Vent marked with red star.

The reasons why such an intense seismic swarm was associated with this particular explosion are poorly understood and therefore of interest. We investigate this eruption to understand this intense seismic activity in more detail and to understand why this large vulcanian explosion occurred at the onset of a phase of lava extrusion. In this study, we use seismic data from the entire precursory swarm to characterize changes in behavior. We apply spectral and multiplet analysis techniques to seismic data preceding the July 2008 vulcanian explosion at SHV to relate these observations to models of volcanic behavior and subsurface processes. Our aim is that our analysis might be compared to other similar volcanic systems worldwide with relatively ease. Therefore, we use readily available monitoring data (seismic, SO_2, and visual observations) and a simple parameterization approach that would be available to most volcano observatories, to relate monitoring observations to subsurface interpretations, and to elucidate volcanic processes that culminated in the vulcanian explosion. We also use multiplet analysis to investigate LP and hybrid classification at SHV to allow us to assess the validity of these as separate earthquake classifications.

2. Prior Constraints on 29 July 2008 Vulcanian Explosion

The vulcanian explosion on 29 July 2008 occurred after a period of increased unrest that began with a small VT swarm on 27 April 2008. During May and June 2008, there were a number of ash-venting episodes, some preceded by VT seismicity [*Cole et al.*, 2014a, 2014b]. Six ash-venting events were observed on 21 July, and a short hour-long period of intense eruptive activity began at 13:35 UTC on 27 July with a series of short ash-venting

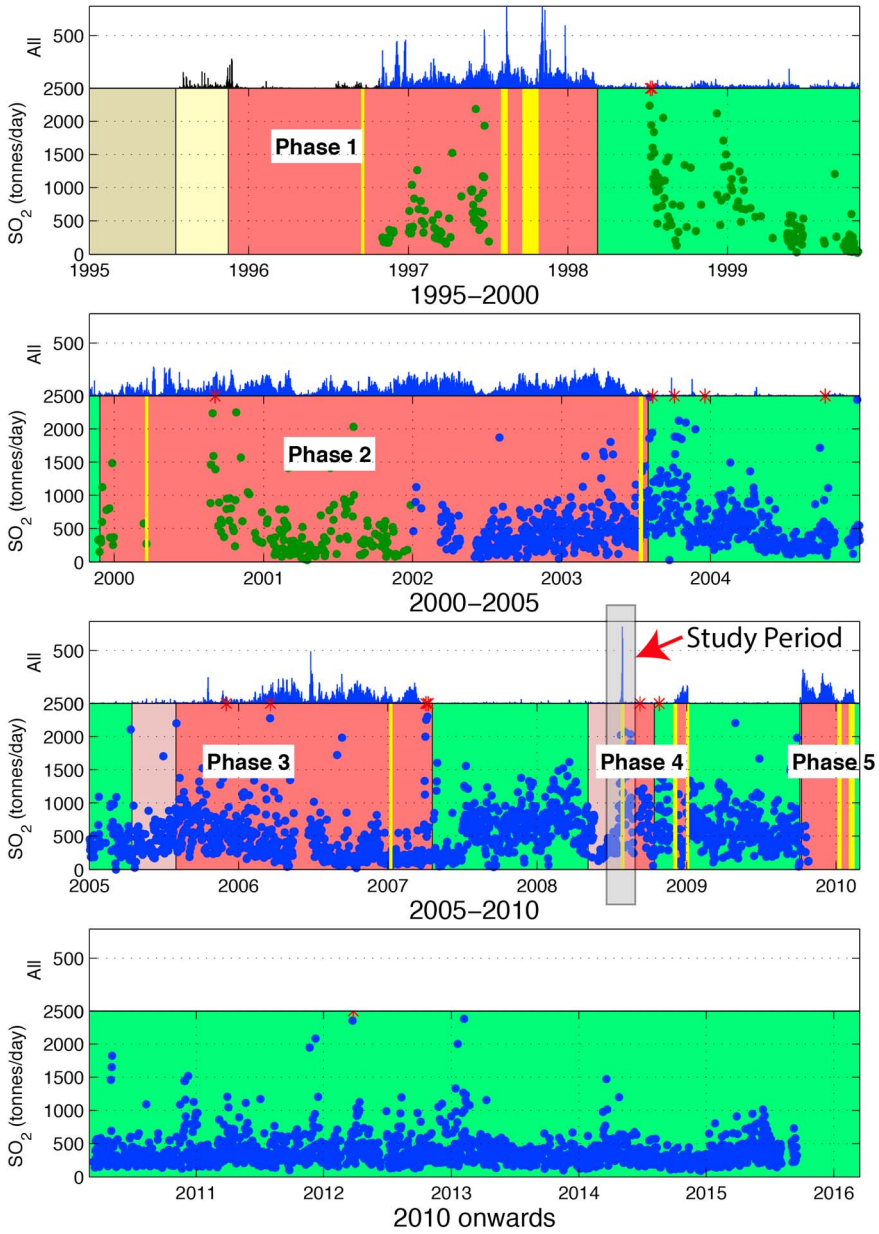

Figure 2. The 1995–2016 timeline of eruptive activity (the pink sections indicate extrusive Phases 1–5, the yellow sections indicate major explosions, and the green sections indicate pauses), total volcanic earthquakes counts (the black vertical bars indicate analogue short period network pre-Oct 1996; the blue vertical bars indicate digital broadband network post-Oct 1996), and SO_2 (the blue dots indicate DOAS network; the green dots indicate COSPEC measurements; the red stars indicate SO_2 values above 2500 t/d that are not plotted). Approximate study period marked by grey box.

events with eruption columns reaching ~2.5 km above sea level [*Cole et al.*, 2014a; *Montserrat Volcano Observatory Open File Rep* (*MVO-OFR*), 2008]. On 29 July at 03:32 UTC a large vulcanian explosion occurred. This eruption released a significant quantity of pumiceous ash and tephra, and the associated plume reached 12 km asl (above sea level), generating pyroclastic flows that traveled ~3.5 km and reached the town of Plymouth [*Cole et al.*, 2014a]. The dense rock equivalent volume of ejecta was estimated at 1.4×10^6 m^3 [*Komorowski et al.*, 2010; *Cole et al.*, 2014a]. The SO_2 plume was detected by Ozone Monitoring Instrument 14 h later at 8 km asl; the explosion released 2.4 kt SO_2 [*Carn and Prata*, 2010; *Hayer et al.*, 2016].

The strain signal from a network of four borehole strainmeters showed a 6 min precursory phase immediately before the explosion and a linear change in strain during the eruption that lasted about 5 min. Modeling of

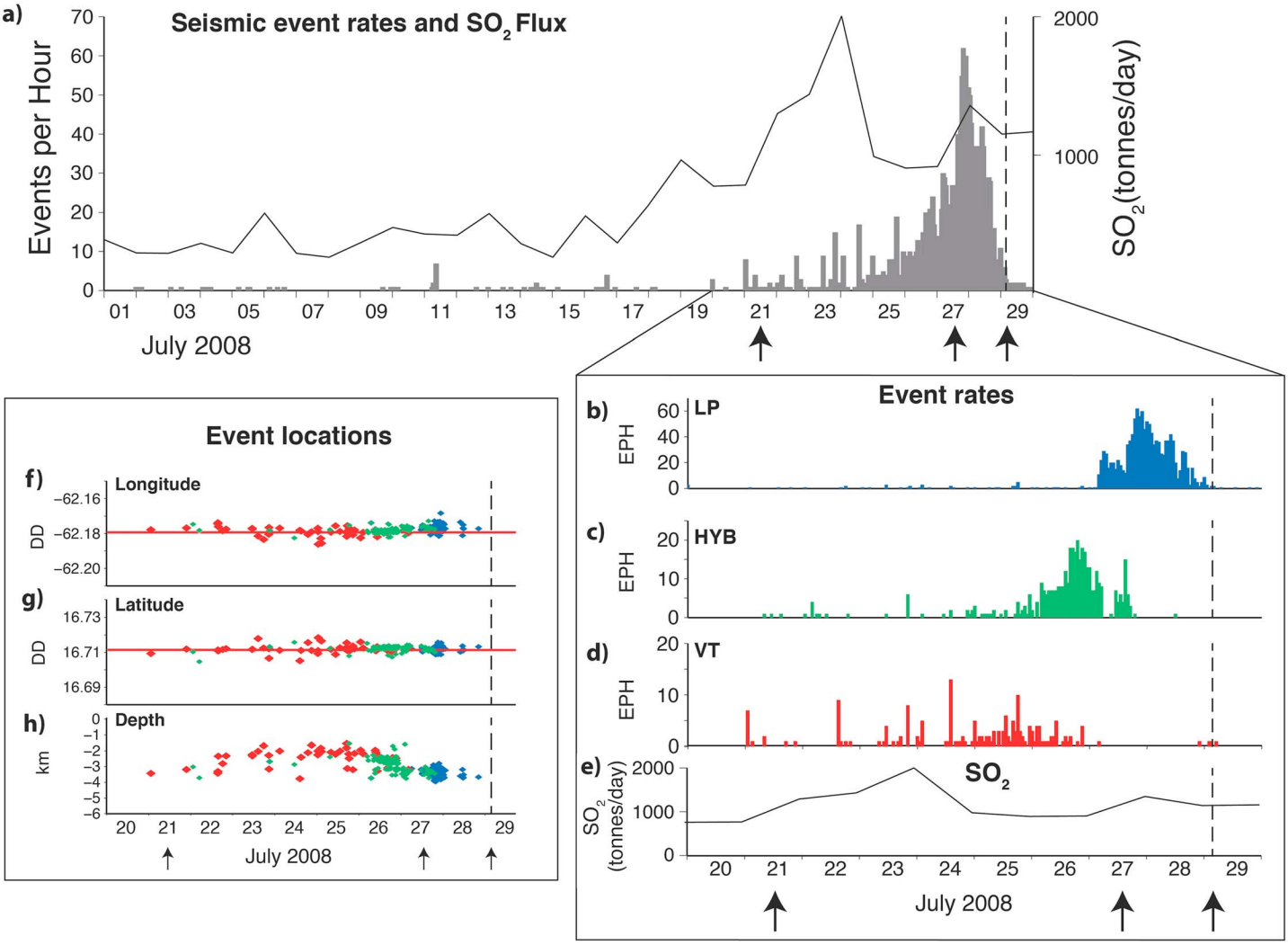

Figure 3. (a) Total seismic events per hour (grey vertical bars) and daily mean SO_2 flux (black solid line) from 1 to 29 July. SO_2 data taken from *Nicholson et al.* [2013]. Errors in SO_2 measurement −10 to +30% [*Edmonds et al.*, 2003]. Events per hour from 20 to 29 July for (b) LP (blue), (c) hybrid (green), and (d) VT (red) events. (e) SO_2 flux (black solid line) from 20 to 29 July. High-quality MVO event locations (horizontal uncertainties of <0.5 km and vertical uncertainties of <1 km): (f) longitude, (g) latitude, and (h) depth below summit of all events between 20 and 29 July with event classifications highlighted in same color scheme as Figures 3b–3d. The horizontal red line in Figures 3f and 3g indicates location of Gages Vent (16.7106°N, 62.1790°E). The black arrows under time axes indicate ash-venting and explosive periods, including the vulcanian explosion on 29 July 2008 (also indicated by dashed vertical line).

the volumetric strain by *Young and Gottsmann* [2015] gave a best fit model that implied a net contraction of about 0.1×10^6 m^3 of an ~40 m radius conduit that was 1.5 ± 0.3 km in length.

Komorowski et al. [2010], citing *Komorowski et al.* [2008], presented SEM images of the eruption products and report that the ash-venting episodes in May 2008 contained 5–10% microvesicular pumice rich in hornblende, along with 10–20% hydrothermally altered products including vapor-phase and hydrothermal precipitates (silica and pyrite). In contrast, the 29 July products included hornblende with 100 μm thick breakdown rims, abundant tabular plagioclase microlites, and occasional vapor-phase cristobalite. The amphibole textures could be interpreted to reflect thermal breakdown of amphiboles, for example, as a consequence of heating by a more mafic magma [e.g., *Devine et al.*, 1998; *Rutherford and Devine*, 2003], although an analysis of the breakdown rim mineralogy is required to confirm this interpretation [e.g., *De Angelis et al.*, 2015]. On Montserrat, the typical stability range inferred for the amphiboles is $P >$ 115–130 MPa, and temperatures of 820–840 °C [e.g., *Barclay et al.*, 1998]. *Komorowski et al.* [2010] also noted the "conspicuous abundance" of mafic enclaves in 29 July ejecta, concluding that there was evidence for gas-rich magma deeper in the conduit immediately prior to this eruption.

In their analysis of long-term rates of degassing on Montserrat, *Nicholson et al.* [2013] saw a strong decrease in both amplitude and dominant period of the gas flux from April to July 2008, which they interpreted as conduit sealing. A similar feature is also seen over the few months before vulcanian explosions in December 2002 and June 2005 [*Nicholson et al.*, 2013].

Following the July explosion, lava extrusion began in early August 2008; SO_2 degassing fluxes remained elevated, averaging 900 t/d until November 2008, and over the course of Phase 4a, a total of 39×10^6 m^3 of magma was erupted, at an average extrusion rate of 2.9 m^3 s^{-1} [*Wadge et al.*, 2014]. *Cole et al.* [2014a] interpreted the products of the explosion as typical "conduit-derived magma." Banded pumice was found in the eruption products, and basaltic to andesitic enclaves were found throughout Phases 4 and 5 [*Plail et al.*, 2014].

These observations place a number of constraints on the system, which are relevant to our work:

1. There is evidence for the presence of some fresh magma in the conduit by May 2008.
2. There is no strong evidence for the depth of origin of the July 2008 magma.
3. The SO_2 release during the explosion was moderate and equivalent to ~8 days of preeruptive degassing or ~3 days of posteruptive degassing. This quantity of gas is consistent with a model of accumulation of gas within a sealed conduit.

3. Data Analysis

3.1. Event Detection and Location

Event-detected seismic waveforms from the MVO network of 11 stations for July 2008 were analyzed. During this time nine three-component broadband stations and two single-component (vertical) short-period stations were operational (Figure 1). MVO uses a standard STA/LTA triggering algorithm, implemented by the real-time seismic analysis software package Earthworm, to detect volcanic events and these were located by MVO using the program HYPOCENTER [*Lienert and Havskov*, 1995] with a 1-D velocity model. Only high-quality earthquakes were selected for further analysis with azimuthal gap of $\leq$185°, RMS of $\leq$0.2 s, and horizontal and vertical uncertainties (as output by HYPOCENTER) of $<$1 km.

3.2. Event Classification

Classification of events was taken from MVO analyst classifications: long-period (LP), volcano-tectonic (VT), hybrid, rockfall and LP-rockfall classes, based on waveform and spectral properties across multiple stations [*Miller et al.*, 1998]. VT events have an impulsive onset with distinct *P* and *S* wave arrivals and frequency content mostly above 5 Hz. LP events have emergent onsets, frequency content below 5 Hz, often have weak *P* wave arrivals, and lack *S* wave arrivals. Hybrid events contain features of both VTs and LPs and are identified by having a high-frequency impulsive onset followed by a low-frequency coda. Rockfall and LP-rockfall events are more typically associated with phases of dome growth [*Calder et al.*, 2002], and as this study period precedes the onset of active extrusion we chose to exclude the minimal numbers of rockfall and LP-rockfall events from further analysis.

3.3. Spectral Analysis

Seismic waveforms were filtered between 0.8 and 20 Hz to remove microseisms ($<$0.8 Hz) and wind noise ($>$20 Hz). Dominant frequencies of each waveform were calculated by taking the fast Fourier transform of a 20 s window (8 s before and 12 s after) around the largest-amplitude peak. Ratios of high- to low-frequency energy ("band-ratios") were calculated from the average spectral amplitudes in frequency bands 1–5 Hz (LF) and 5–9 Hz (HF), and the $\log_2$ of this ratio was calculated [*Rodgers et al.*, 2015b]. A threshold of 5 Hz was chosen for the band-ratio analysis based on the conventional 5 Hz threshold from *Lahr et al.* [1994]. Other thresholds were tested, but there was very little change to the overall temporal pattern and resulted in only an upward or downward shift in the band-ratios. By using a $\log_2$ scale the negative and positive ratios give an equal indication of the relative amounts of high and low energy, with a value of 0 indicating equal high-to-low-frequency energy, -1 indicating twice as much low-frequency energy, and 1 indicating twice as much high-frequency energy.

3.4. Multiplet Analysis

Families of repeating earthquakes (or multiplets) were identified through cross correlation of all earthquakes with all other earthquakes between the start of the seismic crisis phase (24 July) until the end of the explosive

phase (29 July 2008). Seismic waveforms were cross correlated at individual stations by using the entire waveform (using a window of 8 s before and 12 s after the largest-amplitude peak in the waveform). For two events to be considered connected they had to have a cross-correlation threshold of at least 0.7. This 0.7 cross-correlation threshold was chosen from the analysis of the frequency distribution of cross-correlation coefficients. The percentage of cross-correlation coefficients above 0.7 varies from 6% at station MBLG to 32% at station MBBY, with an average of 22%. Multiplets from an individual station (termed "station-multiplets") were identified iteratively via graph theory [*Rodgers et al.*, 2015a]. In this method a master event is identified as being the event that correlates with the most other events in the graph. The master event and all its connected events are grouped into a multiplet and extracted. The graph is then reordered, and the process is repeated until all connected events are extracted. The two largest multiplets, in terms of number of individual events within the multiplet, were compared across the eight most reliable stations (MBBY, MBFL, MBFR, MBGB, MBGH, MBLG, MBRY, and MBWH) to identify the two most robust multiplets across the network (termed "network-multiplets").

4. Results

4.1. Event Rates and Locations

Event rates and locations change noticeably in the few days before the vulcanian explosion on 29 July (Figure 3). Overall event rates are low until 21 July when swarms of VT events start to appear (Figure 3d). These VT events are clustered around the summit. VT hypocenter locations have an average ~0.3 km horizontal distance from Gages Vent (the probable source of the explosion; Figure 1), with a maximum horizontal distance of 1.2 km from Gages Vent (horizontal errors < 0.5 km) (Figures 3f and 3g), and an average depth below summit of 2.4 km, between a range of 1.6 km and 3.9 km (vertical errors < 1 km, summit elevation taken as 0.951 km asl) (Figure 3h). During the higher VT event rates of 24–26 July the depth of VT events clusters at ~2 km depth below summit. VT events continue until 27 July. As VT event rates start to decrease on 25 July, hybrid event rates increase, reaching a peak of 20 events per hour on 26 July (Figure 3c). Hybrid events are slightly deeper than the VTs, with an average depth of 2.9 km between a range of 1.6 km and 3.9 km. Hybrid events have an average horizontal spread of 0.3 km from Gages Vent, with a maximum distance of 0.7 km. Shortly after the peak hybrid rate the LP event rate starts to increase, reaching a maximum of 62 events per hour at 20:00 UTC on 27 July (Figure 3b). Note that event rates were sufficiently high during this peak event rate that it is likely that overlapping earthquakes were missed, and therefore, this peak event rate is probably an underestimate of the true event rate. LP events are deeper than hybrid events, with an average of 3.5 km depth between a range of 2 km and 4 km. Given the lack of *S* wave picks for LP events, depths are likely to be deeper than for those with *S* wave picks; therefore, we treat these apparent deeper events with caution. LP events have a horizontal spread of on average 0.3 km with a maximum distance of 1.2 km from Gages Vent. After the peak in overall event rates at 20:00 UTC on 27 July (which is dominated by the LPs), event rates decreased during the 31 h prior to the vulcanian explosion at 03:32 UTC on 29 July. Inspection of continuous data from helicorder plots shows this to be a real decrease in event rate and not an artifact of individual earthquakes merging into continuous tremor during this time. SO_2 flux during early-mid-July 2008 was ~300 t/d. SO_2 fluxes reached ~2000 t/d on 23 July 2008. Another smaller peak accompanied the peak in seismic event rate (mainly LPs) between 26 and 28 July. There is a slight decrease in SO_2 flux immediately before the explosion, although this decrease is likely to be within the error of the acquisition system. However, we note that there was no large increase in SO_2 flux immediately before the explosion.

4.2. Spectral Analysis

Spectral analysis of the data shows changes in spectral content of individual waveforms in the lead up to the eruption. During early-mid July the frequency content of individual waveforms shows no predominant frequency content, which would be expected due to the lower event rates and dominance of VT events (Figures 4a–4c). During the seismic swarm that begins on 25 July, there are notable changes in frequency content that can be seen from both dominant frequency and band ratio plots (Figure 4). This change is especially visible in the band ratios where there is an overall decrease in frequency content, from ~ -1 on 25 July to ~ -3 until early on 28 July. Peak event rate occurs at 20:00 UTC on 27 July, and approximately 12 h after this peak event rate the frequency content of individual waveforms moves toward higher frequencies until the eruption early on 29 July. As expected VTs have overall higher dominant frequencies, higher band ratios

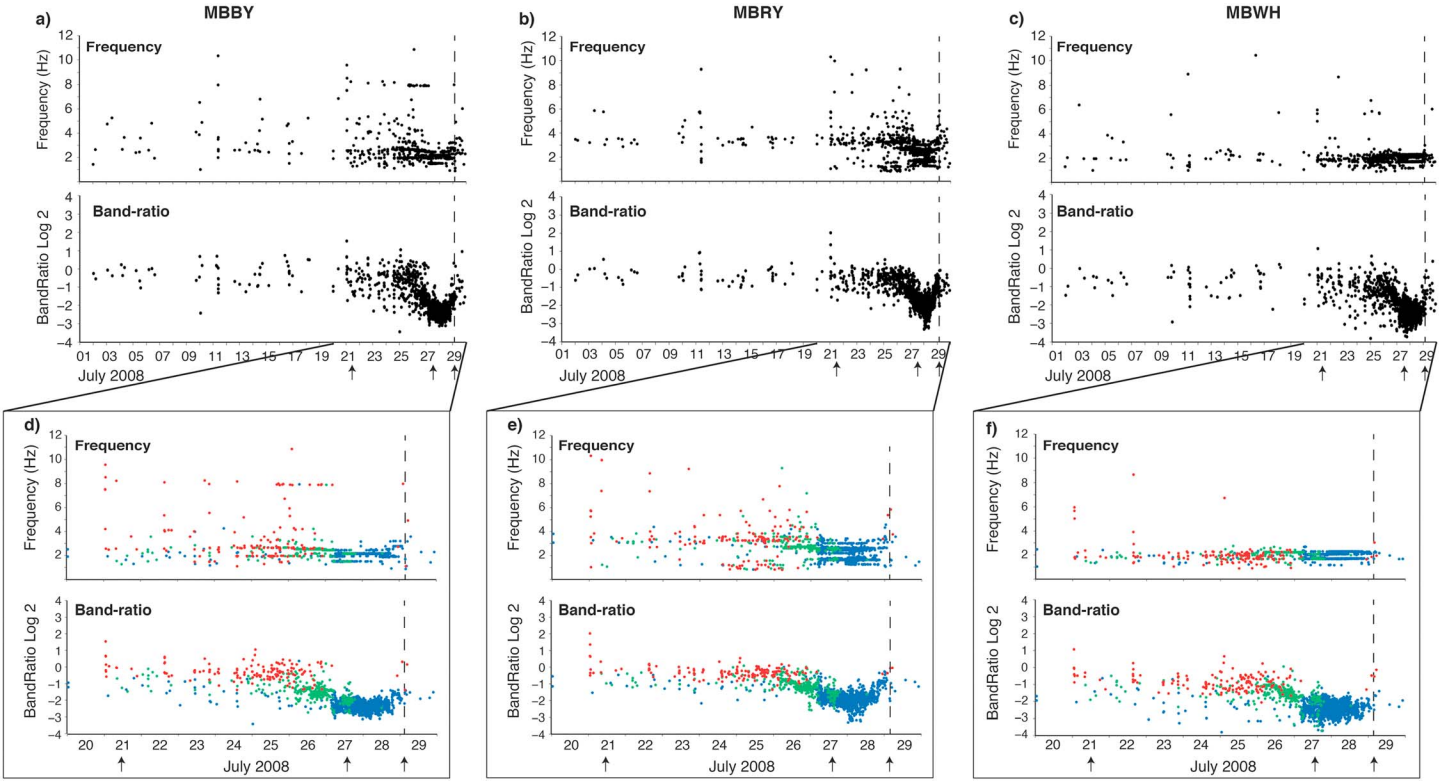

Figure 4. Dominant frequency and band ratio for all events between 1 and 29 July for station (a) MBBY, (b) MBRY, and (c) MBWH. Dominant frequency and band ratio for VT, LP, and hybrid events between 20 and 29 July with event classification highlighted in color (red indicate VT, green indicate hybrid, and blue indicate LP) for station (d) MBBY, (e) MBRY, and (f) MBWH. The black arrows under time axes indicate ash-venting and explosive periods, including the vulcanian explosion on 29 July 2008 (also indicated by dashed vertical line).

(Figures 4d–4f), and more scattered spectral content than the low-frequency events (LPs and hybrids). Spectral content, as shown by band ratios, indicates that the frequency content of the hybrid events decreases over time, with a smooth transition from hybrid events to LP events. Examination of continuous data shows no evidence of rapid changes in frequency (e.g., gliding spectral lines), indicating that the frequency changes we observe are the result of slow processes occurring over hours to days rather than minutes to hours.

4.3. Multiplet Analysis

Multiplet timelines are plotted by ordering multiplets by the time of the first arrival of the first earthquake within a multiplet (Figure 5). From 24 to 26 July no single multiplet dominates the sequence. On 26 July, the second largest multiplet in the catalogue, in terms of number of earthquakes of both station- and network-multiplets, appears (named Multiplet B; Figures 5a–5c). At stations MBWH and MBRY (and on six other stations not shown here) this multiplet dies out at around 06:00 UTC on 27 July, and at approximately the same time Multiplet A, the largest multiplet of the catalogue, begins (Figures 5a–5c). Coincident with this change in multiplet behavior there is a marked increase in event rate that is easily visible on helicorder plots [*MVO OFR*, 2008]. The true event rate is probably higher than that documented in Figure 3a, as event detections may have missed some earthquakes due to the high event rate and merging of earthquakes.

On almost all stations the two largest multiplets (A and B) are separated (Figures 5b and 5c); however, on one station (MBBY; Figure 5a) we observe that these multiplets are connected: i.e., at MBBY earthquakes from Multiplets A and B are all connected to the same master event. The changing cross-correlation coefficients (Figures 6b and 6c) show that for stations MBRY and MBWH the waveform evolves to such an extent that the multiplet splits. Cross-correlation coefficients increase over time until the master event occurs, after which coefficients decrease such that earthquakes in the first multiplet (Multiplet B) are no longer correlated

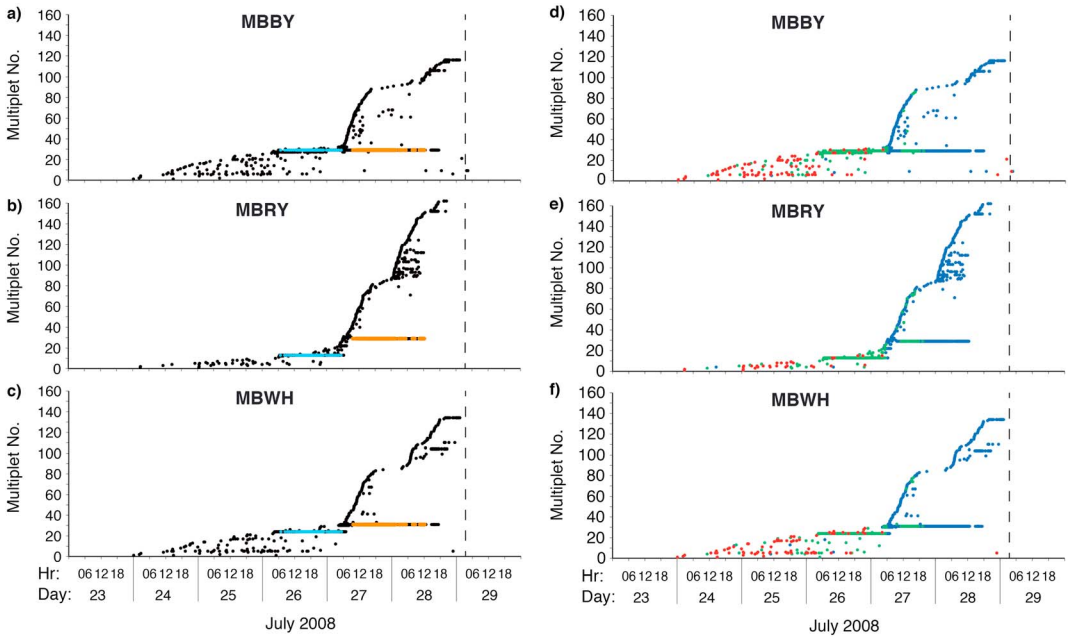

Figure 5. Multiplet timeline between 24 and 29 July with the two largest network-multiplets highlighted in color (pale blue indicate Multiplet B—second largest multiplet and orange indicate Multiplet A—largest multiplet) from stations (a) MBBY, (b) MBRY, and (c) MBWH. Multiplet timeline between 24 and 29 July with event classifications highlighted in color (red indicate VT, green indicate hybrid, and blue indicate LP) from stations (d) MBBY, (e) MBRY, and (f) MBWH. The dashed vertical line denotes vulcanian explosion on 29 July 2008.

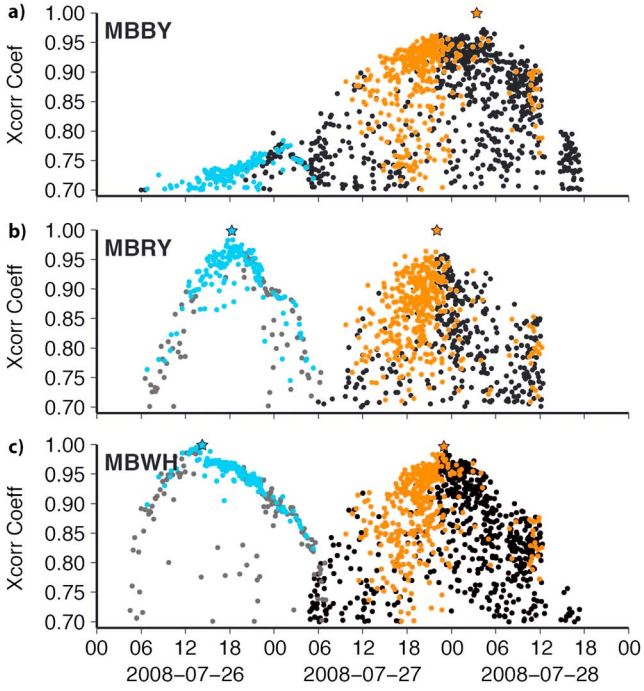

Figure 6. Cross-correlation coefficients over time for largest (black dots) and second largest (grey dots) station-multiplets on stations (a) MBBY, (b) MBRY, and (c) MBWH. N.B there is no second largest multiplet for MBBY. Orange indicate network-multiplet A. Blue indicate network-multiplet B. Master event of each multiplet shown as orange or blue star.

above the threshold to the master event. At this point a new master event is found and a new multiplet is created (Multiplet A), with a similar temporal variation in cross-correlation coefficients. At station MBBY, the waveform also evolves over time (Figure 6a), but the cross-correlation coefficients remain above the threshold for the duration of the multiplet, such that no new multiplet is formed. Signal-to-noise ratios vary across the stations (Figure 7), and visual inspection of these earthquakes shows that MBBY has the best signal-to-noise ratio, suggesting that at MBBY the master event remains better correlated to all events in the multiplet.

For most stations many, but not all, events in Multiplet B are classified as hybrid and similarly many, but not all, events for Multiplet A are classified as LPs (Figures 5d–5f). There are LP events toward the end of Multiplet B and hybrid events toward the beginning of Multiplet A. At station MBBY where Multiplets A and B appear as the same multiplet on this station, there is a clear

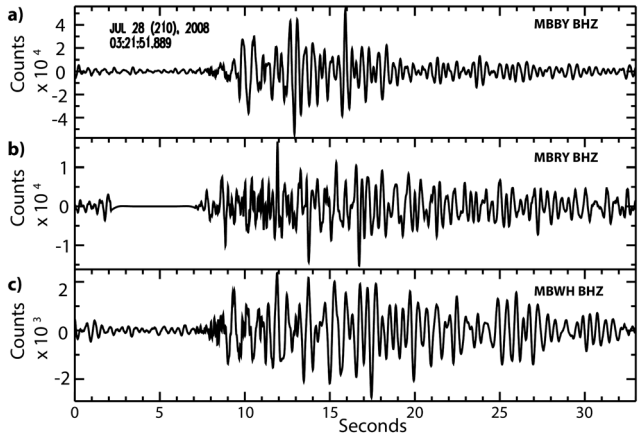

Figure 7. Master event of largest multiplet at station MBBY shown for stations (a) MBBY, (b) MBRY, and (c) MBWH. This event belongs to the largest multiplet at all three stations. All waveforms are filtered between 0.8 and 20 Hz.

transition from hybrid events into LP events within this multiplet (Figure 8). In the multiplets that contain both hybrids and LPs a high-frequency onset is visible for the hybrid events, while the LP events have a low-frequency emergent onset; however, the coda of these earthquakes is highly similar (Figure 8). The cross-correlation coefficients of these waveforms are dominated by the high-amplitude part of the coda (e.g., between ~5 and 12 s on Figure 8), such that the low-amplitude onset can vary slightly and yet the waveform can still be considered part of the same multiplet. The rate of new multiplet formation increases suddenly after ~06:00 UTC on 27 July and continues on most stations until the explosion on 29 July.

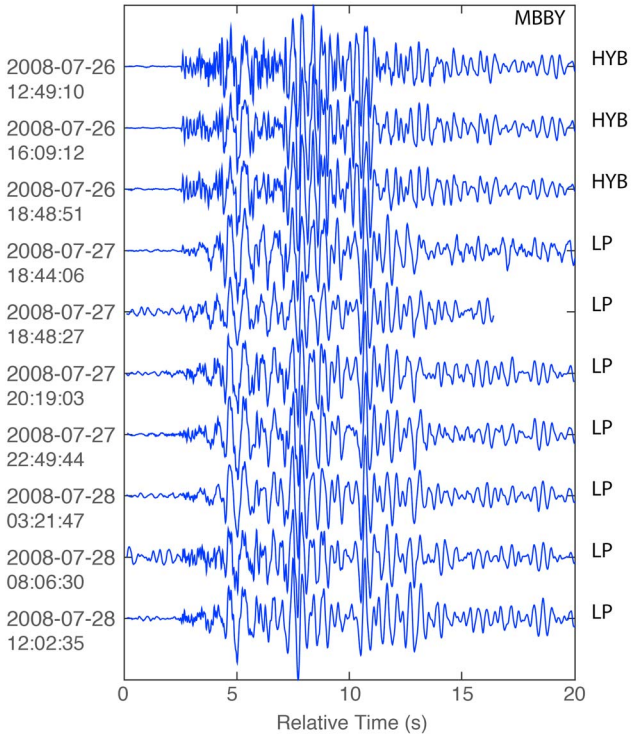

Figure 8. Example waveforms from the dominant multiplet at station MBBY. All waveforms are filtered between 0.8 and 20 Hz and are normalized. MVO analyst classifications are indicated: HYB = hybrid, LP = long period.

5. Discussion

5.1. Classification: Hybrids Versus LPs

We observe multiplets that contain both hybrid events and LP events (Figures 5d–5f and 8). On station MBBY we observe a single large multiplet (Figure 5d) that transitions from hybrid events at the beginning of the multiplet to LP events at the end (Figure 8). The cross-correlation calculation of these waveforms is dominated by the high-amplitude section of the coda, allowing the relatively low-amplitude onset to vary slightly while still remaining within the correlation threshold, and therefore remaining within the same multiplet. We observe hybrids and LPs in the same multiplet that have the same high-amplitude coda, with only slight differences in their onset (Figure 8). For a repeating waveform (i.e., within the correlation constraints to form a multiplet family) to be generated, the same source process must occur repeatedly within the same source volume [*Geller and Mueller*, 1980]. That we observe hybrids and LPs in the same multiplet

suggests that these earthquakes have similar source processes, but with perhaps subtle changes in the initial triggering process, or small changes in event location. Additionally, a smooth transition from hybrid events to LP events during the progressive loss of higher-frequency content (or gain of low-frequency content) (Figure 4) may represent transition between end-members of a spectrum of processes.

This result supports the observation of *Neuberg et al.* [2000], who suggest that hybrids and LPs can be considered end-members of a continuum of signals, at least at SHV. The variation in the onset of the waveform may reflect subtle differences in the triggering mechanism, e.g., slight changes in depth and therefore path [*De Angelis*, 2009], or changes to magma properties [*White et al.*, 1998]. The codas of the waveforms remain correlated, suggesting that the same resonator (magma conduit/column) is being activated [*Neuberg et al.*, 2006]. This is similar to the results of *Ottemöller* [2008], who noted that a high degree of correlation between earthquakes in a hybrid swarm preceding the 2003 dome collapse event was dominated by correlation of the low-frequency coda of the earthquakes, rather than the high-frequency onset.

Hybrid and LP events are often separated in classification schemes at volcanoes [*Lahr et al.*, 1994], but our observations suggest that the usefulness of treating hybrid and LP events as separate event classes should be assessed globally and that multiplet analysis is a useful tool for such assessment. Following previous authors [*Neuberg et al.*, 2000], we refer to hybrids and LP events at SHV together as low-frequency (LF) events in the following sections.

5.2. Comparison of VT Data With Subsurface Models

VT earthquakes are thought to represent shear failure of rock in response to stress change [*Lahr et al.*, 1994]. Stress changes can be related to intrusion of magma [*Roman and Cashman*, 2006], or transport of volatiles [*Jolly and McNutt*, 1999]. Shear-induced failure can result from increases in pore fluid pressure that lower the effective normal stress and promote shear failure [*Byerlee*, 1978]. Such pore fluid pressure changes can be on the order of seconds to days [*Farquharson et al.,* 2016] and can be triggered by degassing or changes in the hydrothermal system [*Jolly and McNutt*, 1999]. *Huppert and Sparks* [2016] model the mass flux, conduit radius, permeability, and viscosity for an ascending compressible fluid in a porous medium, applicable to gas ascending from a shallow magma chamber. Their model suggests that VTs may occur in a critical overpressure zone of failure at approximately two thirds of the vertical distance between the origin of the fluid (e.g., the top of a shallow magma chamber) and the free surface where lithostatic pressure becomes zero (e.g., the top of the edifice). It has been argued that a separate gas phase may exist at SHV, formed as gas separates from melt in the upper magmatic system [*Christopher et al.*, 2015; *Nicholson et al.*, 2013]. Strain data from SHV suggest that the ascent of magmatic gas and volatiles can be decoupled from the ascent of magma and support the model that magmatic gas and volatiles can be rapidly released and ascend from stored gas pockets [*Hautmann et al.*, 2014].

We observe VT hypocenter depths on average ~2.5 km depth below the summit and horizontally tightly clustered (0.4 km) around Gages Vent (Figures 3f–3h). At SHV, the upper limit of the inferred shallow magma chamber is estimated to be around 6–7 km below the summit, although the authors note that magma chamber geometries are not well constrained [*Wadge et al.*, 2006; *Paulatto et al.*, 2012]. *Huppert and Sparks*'s [2016] model predicts that for a magma chamber at 6 km depth, VT hypocenter depths will occur in a critical overpressure zone at ~2 km depth (i.e., two thirds of the magma chamber to surface distance), where overpressures caused by fluid ascent can promote failure on microfaults already close to failure. Our observation of hypocenters with an average of ~2.5 km depth is consistent with this model, given errors in both hypocenter locations and estimates of magma chamber locations. We also note that VT hypocenter depths, in general, at SHV are between 1 and 4 km throughout the eruption history [*Smith*, 2013]. We highlight a small series of ash-venting events on 21 July that occur at the beginning of the VT swarm and during an increase in SO_2 flux, that is consistent with models of decoupled magmatic fluid/gas ascent [*Christopher et al.*, 2015; *Hautmann et al.*, 2014]. Short swarms of VTs (VT strings) have been observed at SHV since 2007, during pauses and precursory phases, but not during extrusion [*Smith*, 2013]. Some of these VT strings have occurred coincident with increased SO_2 flux and ash-venting events, and authors have suggested that such VT seismicity may be driven by gas release [*Smith*, 2013; *Christopher et al.*, 2015]. Therefore, we suggest that the ascent of decoupled magmatic fluid/gas triggered VT seismicity in a critical overpressure failure zone at ~2.5 km depth (Figure 9a).

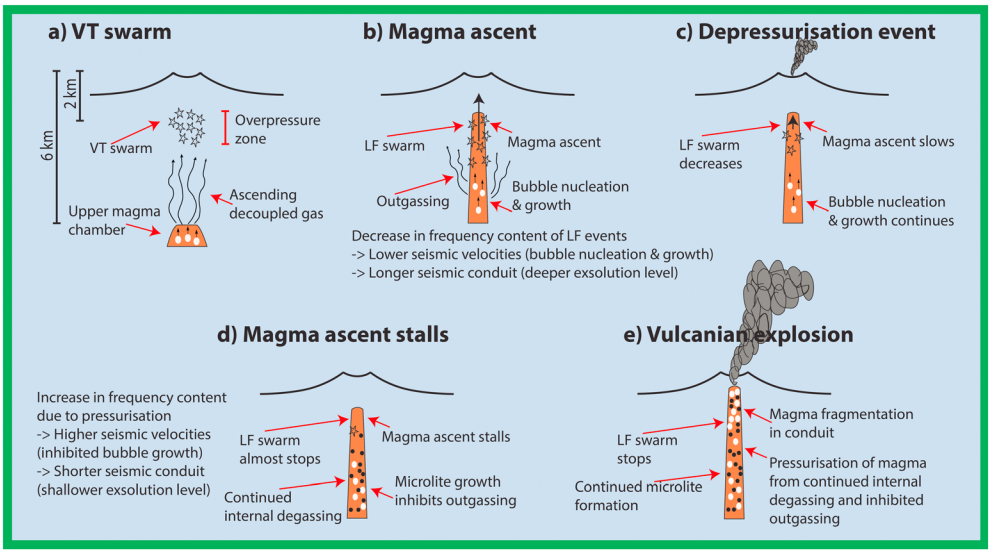

Figure 9. Model of precursory volcanic processes for the July 2008 vulcanian explosion. Initial (a) VT swarm was located in critical overpressure zone caused by volatile release from upper magma chamber. LF swarm during (b) magma ascent was coincident with a decrease in seismic frequency content, due to lowering of seismic velocities and/or longer effective seismic conduit. Rapid (c) depressurization from an ash-venting episode on 27 July 2008 triggered rapid microlite growth and an increase in viscosity that resulted in (d) stalling of magma ascent. Continued internal degassing and inhibited outgassing (due to microlite growth) results in pressurization of the magmatic system and subsequent increase in seismic frequency content, resulting in the final (e) vulcanian explosion on 29 July 2008.

5.3. Comparison of Low-Frequency Seismicity With Subsurface Models

5.3.1. Summary of Existing Models of LF Behavior

LF wave generation in silicic systems such as SHV can be modeled as a trigger followed by resonance produced by an interface wave (sometime termed slow wave or crack wave) at a boundary with an impedance contrast between gas-rich magma and solid rock [*Biot*, 1956; *Ferrazzini and Aki*, 1987; *Chouet*, 1988; *Neuberg et al.*, 2000]. LFs may be triggered by brittle magma fracture at conduit margins [*Tuffen and Dingwell*, 2005], due to high strain rates within a seismogenic window in the conduit, below which magma ascends via ductile flow and above which magma ascends via aseismic plug flow [*Neuberg et al.*, 2006]. *Rowe et al.* [2004] suggest that LF events during the 1996 SHV dome growth episode were triggered by rapid bubble formation and repeated development and destruction of fluid-filled cavities within an ascending magma column. At other dome-forming eruptions, such as Redoubt, Alaska (1989), and Galeras, Colombia (1991), repeated pressurization of a crack and choked flow of fluid through a constriction have been suggested as the mechanisms for the triggering and generation of LF events, in particular monochromatic "Tornillos" [*Gil Cruz and Chouet*, 1997; *Chouet et al.*, 1994].

Once an LF event has been triggered, interface waves travel up and down the boundary, or walls, of a conduit and reflect from the top boundary (e.g., degassed magma plug or dome) and the bottom boundary (e.g., bubble exsolution/nucleation level) [*Neuberg and O'Gorman*, 2002]. These are not organ pipe modes resonating at the acoustic velocity of the magma, but slower interface waves that travel along the boundary of a conduit. The complex wavefield is generated by the radiation of the initial *P* wave, and the interaction of the interface waves with the free surface to generate surface waves [*Jousset et al.*, 2003]. The spectral content of the resulting LF wave is dependent on conduit properties such as the acoustic velocity of the magma, conduit length, and interface properties such as impedance contrast [*Neuberg and O'Gorman*, 2002; *Jousset et al.*, 2003; *Sturton and Neuberg*, 2003, 2006]. A decrease in the acoustic velocity of the magma, e.g., due to bubble nucleation and growth [*Tripoli et al.*, 2016], could result in a slower propagation of interface waves and a lower frequency waveform [*Neuberg and O'Gorman*, 2002]. Decreasing the acoustic velocity of the magma can also reduce the amount of inverse dispersion of the wave and may result in a delay in the higher-frequency part of the wave [*Sturton and Neuberg*, 2006]. Lengthening of the effective seismic conduit length, e.g., via a physical lengthening of

the magma volume during magma ascent, or via changes in the bubble exsolution level due to pressure changes [*Neuberg and O'Gorman*, 2002], could also result in a decrease in seismic frequency content [*Jousset et al.*, 2003]. Cooling of the magma may also result in progressively lower seismic frequency content and would reduce the inverse dispersion of the wavefield [*Jousset et al.*, 2003].

5.3.2. Key Characteristics of LF Swarm Observations

In this section we summarize the key observations of the LF swarm:

1. On 25 July LF earthquake rates increased (Figures 3b and 3c), culminating in one of the most intense seismicity swarms ever observed at SHV (Figure 2).
2. Coincident with an increase in LF event rates, we observe a change in waveform properties. The frequency content of earthquakes decreased (Figure 4), and there was a change in waveform correlation within the dominant waveform family (Figures 5 and 6).
3. A short ash-venting event occurred at 13:35 UTC on 27 July, ~6 h before the peak event rate.
4. Peak event rate of the LF swarm occurred at 20:00 UTC on 27 July (Figure 3a), after which event rates decreased to preswarm levels.
5. Approximately 12 h after peak event rate the frequency content of the waveforms started to increase (Figure 4).

5.3.3. Evidence for Magma Ascent

The observations and models (section 5.3.1) suggest that magma ascent is a key element in the origin of LF seismicity. Therefore, we interpret the intense LF swarm from 25 to 27 July (Figures 3b and 3c) as the final ascent of magma through the shallow conduit system (Figure 9b) [*Hammer and Neuberg*, 2009; *Thomas and Neuberg*, 2012]. The continuous evolution of the seismic waveform of the dominant multiplet of this swarm (Figures 6 and 8) suggests either an evolving source process, changing path effects at all stations, or changing source location. A change in source location is supported by previous analysis of a subset of earthquakes from this swarm, using coda wave interferometry that was interpreted to represent an upward change in source location via magma ascent [*De Angelis*, 2009]. It is also consistent with petrological constraints provided by the erupted products of the July explosion (e.g., the abundance of mafic enclaves) and textural observations that are consistent with the thermal breakdown of amphiboles due to heating by a more mafic intrusion [*Komorowski et al.*, 2010; *Christopher et al.*, 2015] that may reflect the addition of a new pulse of ascending magma. Ash-venting events were observed during the LF swarm and support a model of magma ascent. *Cole et al.* [2014b] interpret syn-extrusive ash venting at SHV as shear-induced fragmentation during periods of high lava extrusion. Although lava extrusion at the surface was not observed until August, such precursory ash-venting events could be associated with migration of magma into the upper conduit.

Magma ascent is consistent with our observation of a concurrent decrease in seismic frequency and an increase in LF event rates. Physical lengthening of the magma volume during magma ascent can lengthen the effective seismic conduit length and could result in lower seismic frequencies [*Jousset et al.*, 2003; *Sturton and Neuberg*, 2006]. Additionally, simultaneous depressurization during magma ascent can also lower seismic velocities (via bubble nucleation and growth due to decompression) and deepen the bubble exsolution level (thereby lengthening the effective seismic conduit length), both of which could lower the frequency content of the waveforms [*Neuberg and O'Gorman*, 2002; *Jousset et al.*, 2003]. Previous models [*Neuberg and O'Gorman*, 2002; *Jousset et al.*, 2003; *Sturton and Neuberg*, 2003, 2006] demonstrate that magma velocities can drop rapidly (e.g., from around 2000 ms^{-1} to 500 ms^{-1} over a 1 h period) during decompression-induced bubble growth and that changes in the bubble exsolution level can lengthen the seismic conduit on the order of many hundreds of meters, which can change frequencies by several hertz. Simultaneous magma ascent and depressurization are not incompatible, as correlation between seismicity and tilt during the 1997 eruption of SHV suggests a magma ascent process, whereby a certain threshold of pressurization results in magma ascent, which then in turn depressurizes the system [*Neuberg et al.*, 2006]. LF event rates would suggest an acceleration of magma ascent until peak event rate (Figures 3b and 3c). Decompression during magma ascent is a viable mechanism for promoting bubble growth during an acceleration of magma ascent. The model we present here is in contrast to the later stages of the swarm (see section 5.3.4). *Sturton and Neuberg* [2003] note that both changes in conduit geometry and changes in magma properties have an effect on the resulting spectral properties of the waveforms, but that the spectra may be more sensitive to changes in magma properties. Our data do

not allow us to separate between physical lengthening of the conduit or depressurization mechanisms; however, both processes are likely to occur simultaneously.

There is an alternative explanation for these observations. Emplacement of hot magma into cooler conduit material would initially have a very sharp thermal gradient. Over time the thickness of this thermal gradient (a "thermal transition zone") would increase at the walls of the conduit as the magma cools from the conduit edges inward. Increasing the thickness of this thermal transition zone at the walls of the conduit would progressively lower seismic frequency content and reduce the inverse dispersion of the wavefield [*Jousset et al.*, 2003]. Our observations do not allow us to distinguish between the mechanisms outlined above. It is possible that a combination of lowering seismic velocities of the magma, deepening of the effective seismic conduit length, and development of a thermal transition zone in the walls of the conduit could all occur during magma ascent. Detailed quantitative modeling would be necessary to test these hypotheses further, and such models will be considered in future work.

5.3.4. Evidence for Magma Stalling and Pressurization

If we take LF event rate as a proxy for magma ascent [*Hammer and Neuberg*, 2009], then the reduction in event rate after the peak (~31 h) before the main explosion may indicate a slowing down or stalling of magma ascent (Figure 9c), where a critical ascent velocity of the magma is needed to sustain a high enough shear stress to produce brittle failure [*Neuberg et al.*, 2006]. We note that a short ash-venting episode occurred at 13:35 UTC on 27 July (~6 h before peak event rate), and we observe the start of an increase in seismic frequency content ~12 h after peak event rate (Figures 3 and 4). One possibility is that the magma began to stall after this ash-venting event, due to an increase in viscosity mediated by depressurization-triggered crystallization (Figure 9d). Previous studies have noted that an increase in viscosity through crystallization and microlite growth can happen quickly in a magma conduit [*Geschwind and Rutherford*, 1995], especially in response to volatile loss and rapid depressurization [*Swanson et al.*, 1989; *Sparks*, 1997; *Hammer et al.*, 1999]. The products of 29 July 2008 explosion were vesicular pumices, with a distinct population of microlites [*Komorowski et al.*, 2010], in contrast to the pumiceous products of earlier vulcanian explosions that were relatively microlite-poor [e.g., *Rutherford and Devine*, 2003].

This depressurization-triggered crystallization process could also account for the increase in seismic frequency content ~18 h after the small ash-venting episode. The rapid magmatic viscosity change induced by development of microlites in the conduit [*Geschwind and Rutherford*, 1995] could in turn plausibly inhibit magma outgassing [*Tait et al.*, 1989], and subsequent continued internal magma degassing could pressurize the system (Figures 9d and 9e). In contrast to the changes in frequency observed during the first part of the LF swarm (see section 5.3.3) the opposite mechanism could be invoked here to explain these changes in frequency. Increasing pressure in the magma conduit would both increase seismic velocity of the magma (due to reduced bubble content) and cause the bubble exsolution level to shallow, resulting in the observed higher seismic waveform frequencies [*Neuberg and O'Gorman*, 2002; *Jousset et al.*, 2003]. *Jousset et al.* [2003] modeled frequency increases at SHV of several hertz by rapidly reducing conduit lengths from 1000 m to 900 m. Small changes in bubble nucleation density can produce significant changes to seismic velocities [*Tripoli et al.*, 2016], and therefore seismic frequencies.

Our new observations of the buildup to this explosive event at SHV in 2008 are consistent with seismic interpretations during other periods of behavior at SHV and at eruptions at other systems. For example, changing pressure conditions has been linked to increasing frequency content of tremor at SHV during the December 1997 eruption [*Neuberg and O'Gorman*, 2002] and changing frequency content during degassing explosions has been linked to changing acoustic velocities of magma at Arenal [*Benoit and McNutt*, 1997]. In contrast, our observations do not support the model discussed in section 5.3.3 on development of a thermal transition zone in the walls of the conduit as slowing of magma ascent would likely increase any thermal transition zone at the conduit edges, resulting in a continued decrease in seismic frequencies rather than the increase in seismic frequency that we observe.

5.4. Precursory Quiescence and Explosion

Precursory quiescence has been observed before vulcanian eruptions in a variety of settings [*Hotovec et al.*, 2013; *Nishimura et al.*, 2013; *Roman et al.*, 2016] and has been attributed to mechanisms such as sealing of a shallow magmatic-hydrothermal system [*Rodgers et al.*, 2013; *Nishimura et al.*, 2013; *Geirsson et al.*, 2014; *Rodgers et al.*, 2015b] or crystallization in a magma conduit preventing magma outgassing [*Fischer*

et al., 1994]. In this instance, the large vulcanian explosion occurred at 03:32 UTC on 29 July, after ~7 h of relative seismic quiescence, especially in terms of VT earthquakes (Figure 3). SO_2 flux at SHV does not increase in the 24 h before the eruption (Figure 3e). We observe a slight decrease in SO_2 flux, but this is likely within the error of the differential optical absorption spectroscopy (DOAS) system. Our observations are consistent with a model of sealing of the magmatic system, either via magmatic crystallization, a magmatic-hydrothermal mechanism, or another mechanism, that prevented external outgassing (Figure 9e). This would then have resulted in a pressurization of the magmatic system [*Stix et al.*, 1997]. Indeed, previous studies have modeled this explosion as the progressive internal failure of an already pressurized magma conduit that evacuated the upper 1.5 km of the conduit [*Gottsmann et al.*, 2011]. The presence of juvenile material in the erupted products [*Komorowski et al.*, 2010] is consistent with a model of pressurization and fragmentation, following an injection of fresh magma into the conduit, and the presence of microlite textures [*Komorowski et al.*, 2010] in the ejecta supports magmatic crystallization as the mechanism for pressurization.

The low rates of seismicity before the eruption may appear inconsistent with a model of increasing pressurization that would predict increasing rates of VT seismicity until failure [*Voight*, 1988]. However, low rates of seismicity during precursory pressurization have been observed at other systems [*Fischer et al.*, 1994; *Nishimura et al.*, 2013; *Roman et al.*, 2016], and although these studies focus primarily on LF events, we note the similar lack of VT seismicity before these eruptions. The low rate of VT seismicity we observed before the July 2008 explosion at SHV (Figure 3d) may be due to the Kaiser effect, whereby rock fracturing does not occur until stress levels have reached a previously attained level [*Kaiser*, 1953; *Lavrov*, 2003]. This effect has been observed at Krafla, Iceland, with respect to ground deformation during repeated episodes of magma intrusion [*Heimisson et al.*, 2015]. The lack of VTs may also reflect the shallow nature of the pressurization source, where material surrounding the upper conduit is too weak to support stress needed for shear failure [*Bean et al.*, 2013]. Alternatively, sealing of the magma outgassing process may reduce pore fluid pressure in the surrounding VT source area, and while pressure may increase inside the magmatic system, the lack of pore fluid pressure may inhibit rock fracture in the surrounding seismogenic zone [*Byerlee*, 1978]. Thus, our observation of precursory quiescence during a period of final pressurization is consistent with previous models of this explosion [*Gottsmann et al.*, 2011] and with models of preeruptive seismic quiescence at other volcanoes globally [*Fischer et al.*, 1994; *Nishimura et al.*, 2013; *Roman et al.*, 2016].

5.5. Comparison to Other Explosions at SHV

There have been over 100 major vulcanian explosions at SHV since eruptive activity began in 1995 [*Cole et al.*, 2014a]. Many of the largest explosions are associated with dome collapse events that mark the end of effusive periods, e.g., the 1997 Boxing Day event, the July 2003 dome collapse, and the February 2010 dome collapse, or dome collapse during effusive periods, e.g., the May 2006 dome collapse event [*Kokelaar*, 2002; *Wadge et al.*, 2014]. Explosions associated with effusion and dome collapse present a very different volcanological and structural setting than those occurring during pauses in dome growth, and direct comparison may not be warranted. Other large explosions have occurred at SHV outside periods of effusion. A vulcanian explosion occurred in December 2008 after a short 2 month pause in effusive activity. This explosion was of similar size to that of the July 2008 explosion; however, unlike the July 2008 explosions it was pumice poor and was not preceded by any notable seismic activity [*Cole et al.*, 2014a]. The July 2008 explosion was generated by evacuation of juvenile material from the conduit, and the intense precursory seismic swarm may indicate processes involved in magma movement and magma pressurization. Perhaps, the unusual presence of microlites in the magma [*Komorowski et al.*, 2010] allowed pressurization of the magmatic conduit during magma ascent, resulting in the vulcanian explosion on 29 July 2008 rather than lava effusion and dome growth from ascending magma, although further investigation is required to explore this hypothesis. The December 2008 explosion shows no such precursory seismic swarm; it destroyed much of the dome, and it has been suggested that it was associated with rapid pressurization of the feeder dyke [*Chardot et al.*, 2010] or sudden pressurization of the deep magmatic system [*Gottsmann et al.*, 2011]. These two explosions represent different precursory conduit processes and explosion mechanisms, and the intense seismic swarm preceding the July 2008 explosion allows us to suggest a model of magma ascent and conduit pressure changes.

6. Conclusion

The July 2008 eruption is one of the largest explosions to mark the onset of an effusive phase of activity at Soufriére Hills Volcano, Montserrat, and is associated with one of the most intense seismic swarms recorded at SHV. We analyzed seismic data from the precursory phase of the July 2008 vulcanian explosion at SHV, to explore the processes occurring during a transition from a period of quiescence to an explosion at a volcano with repeated transitions. We observe a VT swarm concurrent with a series of small ash-venting events, followed by a large low-frequency (LF) swarm and a decrease in spectral content concurrent with the increase in event rates. An ash-venting event a few hours before peak event rate was followed by an increase in spectral content of LF events and concurrent with a decrease in event rates. Seismic quiescence occurred in the final 7 h before the large vulcanian explosion on 29 July 2008. We suggest that the initial VT swarm and ash-venting events indicate initial ascent of decoupled gas ahead of rising magma. The LF swarm and coincident spectral changes suggest that final magma ascent through the upper conduit system occurred over a 2 day period from 26 to 27 July before stalling. An ash-venting event on 27 July may have triggered rapid microlite growth and initiated subsequent pressurization of the magmatic system due to inhibited magmatic outgassing. Spectral changes of LF events suggest that pressurization of the magmatic system may have occurred in the final ~24 h before the vulcanian explosion. Our observation that LP events and hybrid events occur within the same multiplet indicates that these earthquakes have the same (or very similar) source processes and should be considered part of the same classification, at least at SHV. Our results highlight the potential for using detailed spectral analysis to understand the processes occurring within magmatic systems and the transition between quiescence and eruption. Such analyses are achievable by using relatively readily available data and straightforward parameterizations. This should facilitate the analysis of preeruptive spectral changes in seismicity at similar quiescent-explosive transitions at other volcanoes in order to test and explore the wider applicability of this model of magma ascent and pressurization.

Acknowledgments

We thank the staff at the Montserrat Volcano Observatory (MVO) for access to geophysical data, for graciously hosting our visits, and for continued collaboration with the STREVA project. Data used in this study were acquired and archived by MVO and are used under the terms of the data agreement between MVO and M. Rodgers. To access the data used in this study please contact MVO (www.mvo.ms). We thank Steve McNutt, Steve Sparks, and Glenn Thompson for their insightful discussions and advice on this project. In particular, thanks to Glenn Thompson for the advice and help using GISMO. Figure 8 was made by using GISMO correlation toolbox (http://geoscience-community-codes.github.io/GISMO). We thank two anonymous reviewers for carefully reviewing this manuscript and providing constructive comments and suggestions. Work undertaken at Oxford was completed while funded on NERC STREVA grant NE/J020001/1.

References

Barclay, J., M. J. Rutherford, M. R. Carroll, M. D. Murphy, J. D. Devine, J. Gardner, and R. S. J. Sparks (1998), Experimental phase equilibria constraints on pre-eruptive storage conditions of the Soufriere Hills magma, *Geophys. Res. Lett.*, *25*, 3437–3440, doi:10.1029/98GL00856.

Battaglia, J., J.-L. Got, and P. Okubo (2003), Location of long-period events below Kilauea Volcano using seismic amplitudes and accurate relative relocation, *J. Geophys. Res.*, *108*(B12), 2553, doi:10.1029/2003JB002517.

Bean, C. J., L. De Barros, I. Lokmer, J. Métaxian, G. O'Brien, and S. Murphy (2013), Long-period seismicity in the shallow volcanic edifice formed from slow-rupture earthquakes, *Nat. Geosci.*, *7*, 71–75.

Benoit, J. P., and S. R. McNutt (1997), New constraints on source processes of volcanic tremor at Arenal Volcano, Costa Rica, using broadband seismic data, *Geophys. Res. Lett.*, *24*, 449–452, doi:10.1029/97GL00179.

Biot, M. A. (1956), Theory of propagation of elastic waves in a fluid-saturated porous solid. I. Low-frequency range, *J. Acoust. Soc. Am.*, *28*, 168–178.

Bluth, G. J. S., and W. I. Rose (2004), Observations of eruptive activity at Santiaguito volcano, Guatemala, *J. Volcanol. Geotherm. Res.*, *136*, 297–302.

Buurman, H., and M. E. West (2010), Seismic precursors to volcanic explosions during the 2006 eruption of Augustine Volcano, in *The 2006 Eruption of Augustine Volcano, Alaska*, edited by J. A. Power, M. L. Coombs, and J. T. Freymueller, *U.S.G.S. Prof. Pap. 1769*, 41–57.

Buurman, H., M. E. West, and G. Thompson (2013), The seismicity of the 2009 Redoubt eruption, *J. Volcanol. Geotherm. Res.*, *259*, 16–30.

Byerlee, J. (1978), Friction of rocks, *Pure Appl. Geophys.*, *116*, 615–626.

Calder, E. S., R. Luckett, R. S. J. Sparks, and B. Voight (2002), Mechanisms of lava dome instability and generation of rockfalls and pyroclastic flows at Soufriere Hills Volcano, Montserrat, *Geol. Soc. London Mem.*, *21*, 173–190.

Carn, S. A., and F. J. Prata (2010), Satellite-based constraints on explosive SO2 release from Soufriere Hills Volcano, Montserrat, *Geophys. Res. Lett.*, *37*, L00E22, doi:10.1029/2010GL044971.

Cassidy, M., P. D. Cole, K. E. Hicks, N. R. Varley, N. Peters, and A. H. Lerner (2015), Rapid and slow: Varying magma ascent rates as a mechanism for vulcanian explosions, *Earth Planet. Sci. Lett.*, *420*, 73–84.

Chardot, L., et al. (2010), Explosion dynamics from strainmeter and microbarometer observations, Soufriere Hills Volcano, Montserrat: 2008–2009, *Geophys. Res. Lett.*, *37*, L00E24, doi:10.1029/2010GL044661.

Chouet, B. A. (1988), Resonance of a fluid-driven crack: Radiation properties and implications for the source of long-period events and harmonic tremor, *J. Geophys. Res.*, *93*, 4375–4400, doi:10.1029/JB093iB05p04375.

Chouet, B. A. (1996), Long-period volcano seismicity: Its source and use in eruption forecasting, *Nature*, *380*, 309–316.

Chouet, B. A., R. A. Page, C. D. Stephens, J. C. Lahr, and J. A. Power (1994), Precursory swarms of long-period events at Redoubt Volcano (1989–1990), Alaska: Their origin and use as a forecasting tool, *J. Volcanol. Geotherm. Res.*, *62*, 95–135.

Christopher, T. E., J. Blundy, K. Cashman, P. Cole, M. Edmonds, P. J. Smith, R. S. J. Sparks, and A. Stinton (2015), Crustal-scale degassing due to magma system destabilization and magma-gas decoupling at Soufriere Hills Volcano, Montserrat, *Geochem. Geophys. Geosyst.*, *16*, 2797–2811, doi:10.1002/2015GC005791.

Clarke, A. B., T. E. Ongaro, and A. Belousov (2015), Vulcanian Eruptions, in *The Encyclopedia of Volcanoes*, 2nd ed., Elsevier Inc., Acad. Press, Amsterdam.

Cole, P. D., P. J. Smith, A. J. Stinton, H. M. Odbert, M. L. Bernstein, J.-C. Komorowski, and R. C. Stewart (2014a), Vulcanian explosions at Soufriere Hills Volcano, Montserrat between 2008 and 2010, *Geol. Soc. London Mem.*, *39*, 93–111.

Cole, P. D., P. Smith, J.-C. Komorowski, F. Alfano, C. Bonadonna, A. J. Stinton, T. Christopher, H. M. Odbert, and S. Loughlin (2014b), Ash venting occurring both prior to and during lava extrusion at Soufriere Hills Volcano, Montserrat, from 2005 to 2010, *Geol. Soc. London Mem.*, *39*, 71–92.

De Angelis, S. (2009), Seismic source displacement by coda wave interferometry at Soufriere Hills Volcano, Montserrat, WI, *Nat. Hazards Earth Syst. Sci.*, *9*, 1341–1347.
De Angelis, S. H., J. Larsen, M. Coombs, A. Dunn, and L. Hayden (2015), Amphibole reaction rims as a record of pre-eruptive magmatic heating: An experimental approach, *Earth Planet. Sci. Lett.*, *426*, 235–245.
Devine, J. D., M. J. Rutherford, and J. E. Gardner (1998), Petrologic determination of ascent rates for the 1995-1997 Soufriere Hills Volcano andesite magma, *Geophys. Res. Lett.*, *25*, 3673–3676, doi:10.1029/98GL00912.
Diller, K., A. B. Clarke, B. Voight, and A. Neri (2006), Mechanisms of conduit plug formation: Implications for vulcanian explosions, *Geophys. Res. Lett.*, *33*, L20302, doi:10.1029/2006GL027391.
Druitt, T. H., et al. (2002), Episodes of cyclic vulcanian explosive activity with fountain collapse at Soufriere Hills Volcano, Montserrat, *Geol. Soc. London Mem.*, *21*, 281–306.
Edmonds, M., and R. A. Herd (2007), A volcanic degassing event at the explosive-effusive transition, *Geophys. Res. Lett.*, *34*, L21310, doi:10.1029/2007GL031379.
Edmonds, M., R. A. Herd, B. Galle, and C. M. Oppenheimer (2003), Automated, high time resolution measurements of SO2 flux at Soufrière Hills Volcano, Montserrat, *Bull. Volcanol.*, *65*, 578–586.
Farquharson, J., M. J. Heap, P. Baud, T. Reuschlé, and N. R. Varley (2016), Pore pressure embrittlement in a volcanic edifice, *Bull. Volcanol.*, *78*(6), 1–19.
Ferrazzini, V., and K. Aki (1987), Slow waves trapped in a fluid-filled infinite crack: Implications for volcanic tremor, *J. Geophys. Res.*, *92*, 9215–9223, doi:10.1029/JB092iB09p09215.
Fischer, T. P., M. M. Morrissey, V. Marta Lucía Calvache, M. Diego Gòmez, C. Roberto Torres, J. Stix, and S. N. Williams (1994), Correlations between SO2 flux and long-period seismicity at Galeras volcano, *Nature*, *368*, 135–137.
Geirsson, H., et al. (2014), Multidisciplinary observations of the 2011 explosive eruption of Telica volcano, Nicaragua: Implications for the dynamics of low-explosivity ash eruptions, *J. Volcanol. Geotherm. Res.*, *271*, 55–69.
Geller, R. J., and C. S. Mueller (1980), Four similar earthquakes in central California, *Geophys. Res. Lett.*, *7*, 821–824, doi:10.1029/GL007i010p00821.
Geschwind, C. H., and M. J. Rutherford (1995), Crystallization of microlites during magma ascent: The fluid mechanics of 1980–1986 eruptions at Mount St Helens, *Bull. Volcanol.*, *57*, 356–370.
Gil Cruz, F., and B. A. Chouet (1997), Long-period events, the most characteristic seismicity accompanying the emplacement and extrusion of a lava dome in Galeras Volcano, Colombia, in 1991, *J. Volcanol. Geotherm. Res.*, *77*, 121–158.
Gottsmann, J., S. De Angelis, N. Fournier, M. Van Camp, S. Sacks, A. Linde, and M. Ripepe (2011), On the geophysical fingerprint of vulcanian explosions, *Earth Planet. Sci. Lett.*, *306*, 98–104.
Green, D., and J. Neuberg (2006), Waveform classification of volcanic low-frequency earthquake swarms and its implication at Soufrière Hills Volcano, Montserrat, *J. Volcanol. Geotherm. Res.*, *153*, 51–63.
Hammer, C., and J. W. Neuberg (2009), On the dynamical behaviour of low-frequency earthquake swarms prior to a dome collapse of Soufrière Hills Volcano, Montserrat, *Geophys. Res. Lett.*, *36*, L06305, doi:10.1029/2008GL036837.
Hammer, J. E., K. V. Cashman, R. P. Hoblitt, and S. Newman (1999), Degassing and microlite crystallization during pre-climactic events of the 1991 eruption of Mt. Pinatubo, Philippines, *Bull. Volcanol.*, *60*, 355–380.
Harrington, R. M., and E. E. Brodsky (2007), Volcanic hybrid earthquakes that are brittle-failure events, *Geophys. Res. Lett.*, *34*, L06308, doi:10.1029/2006GL028714.
Hautmann, S., F. Witham, T. Christopher, P. Cole, A. T. Linde, I. S. Sacks, and R. S. J. Sparks (2014), Strain field analysis on Montserrat (W.I.) as tool for assessing permeable flow paths in the magmatic system of Soufrière Hills Volcano, *Geochem. Geophys. Geosyst.*, *15*, 676–690, doi:10.1002/2013GC005087.
Hayer, C. S., G. Wadge, M. Edmonds, and T. Christopher (2016), Sensitivity of OMI SO2 measurements to variable eruptive behaviour at Soufrière Hills volcano, Montserrat, *J. Volcanol. Geotherm. Res.*, *312*, 1–10.
Heimisson, E. R., P. Einarsson, F. Sigmundsson, and B. Brandsdóttir (2015), Kilometer-scale Kaiser effect identified in Krafla volcano, Iceland, *Geophys. Res. Lett.*, *42*, 7958–7965, doi:10.1002/2015GL065680.
Hotovec, A. J., S. G. Prejean, J. E. Vidale, and J. Gomberg (2013), Strongly gliding harmonic tremor during the 2009 eruption of Redoubt Volcano, *J. Volcanol. Geotherm. Res.*, *259*, 89–99.
Huppert, H. E., and R. S. Sparks (2016), Compressible vapour flow in conduits and fractures, *J. Fluid Mech.*, *802*, 750–759.
Jolly, A. D., and S. R. McNutt (1999), Seismicity at the volcanoes of Katmai National Park, Alaska; July 1995-December 1997, *J. Volcanol. Geotherm. Res.*, *93*, 173–190.
Jousset, P., J. Neuberg, and S. Sturton (2003), Modelling the time-dependent frequency content of low-frequency volcanic earthquakes, *J. Volcanol. Geotherm. Res.*, *128*, 201–223.
Kaiser, J. (1953), Information and conclusions from the measurement of noises in tensile stressing of metallic materials, *Arch. Eisenhuttenwes.*, *24*, 43–45.
Ketner, D., and J. Power (2013), Characterization of seismic events during the 2009 eruption of Redoubt Volcano, Alaska, *J. Volcanol. Geotherm. Res.*, *259*, 45–62.
Kokelaar, B. P. (2002), Setting, chronology and consequences of the eruption of Soufriere Hills Volcano, Montserrat (1995–1999), *Geol. Soc. London Mem.*, *21*, 1–43.
Komorowski, J. C., Y. Legendre, T. Christopher, R. Stewart, V. Clouard, and P. Joseph (2008), Appendix 2: Preliminary microtextural observations of tephra erupted on 13 May, 28 July and 25 August 2008, in *Report for the Scientific Advisory Committee on Montserrat Volcanic Activity, Prepared for SAC11: 20–22 October 2008*, *MVO Open File Rep. 08/02*, edited by R. Stewart et al., pp. 47–53, Montserrat Volcano Obs., Flemmings, Montserrat.
Komorowski, J. C., et al. (2010), Insights into processes and deposits of hazardous vulcanian explosions at Soufrière Hills Volcano during 2008 and 2009 (Montserrat, West Indies), *Geophys. Res. Lett.*, *37*, L00E19, doi:10.1029/2010GL042558.
Lachowycz, S. M., D. M. Pyle, T. A. Mather, N. R. Varley, H. M. Odbert, P. D. Cole, and G. a. Reyes-Dávila (2013), Long-range correlations identified in time-series of volcano seismicity during dome-forming eruptions using detrended fluctuation analysis, *J. Volcanol. Geotherm. Res.*, *264*, 197–209.
Lahr, J. C., B. A. Chouet, C. D. Stephens, J. A. Power, and R. A. Page (1994), Earthquake classification, location, and error analysis in a volcanic environment: Implications for the magmatic system of the 1989–1990 eruptions at Redoubt Volcano, Alaska, *J. Volcanol. Geotherm. Res.*, *62*, 137–151.
Lamb, O. D., S. De Angelis, K. Umakoshi, A. J. Hornby, J. E. Kendrick, and Y. Lavallée (2015), Cyclic fracturing during spine extrusion at Unzen volcano, Japan, *Solid Earth Discuss.*, *7*, 2109–2149.

Lavrov, A. (2003), The Kaiser effect in rocks: Principles and stress estimation techniques, *Int. J. Rock Mech. Min. Sci.*, *40*, 151–171.
Lienert, B. R., and J. Havskov (1995), A computer program for locating earthquakes both locally and globally, *Seismol. Res. Lett.*, *66*, 26–36.
Loughlin, S. C., P. J. Baxter, W. P. Aspinall, B. Darroux, C. L. Harford, and A. D. Miller (2002), Eyewitness accounts of the 25 June 1997 pyroclastic flows and surges at Soufriere Hills Volcano, Montserrat, and implications for disaster mitigation, *Geol. Soc. London Mem.*, *21*, 211–230.
Major, J. J., and L. E. Lara (2013), Overview of Chaitén Volcano, Chile, and its 2008-2009 eruption, *Andean Geol.*, *40*, 196–215.
McNutt, S. R. (1996), Seismic monitoring and eruption forecasting of volcanoes: A review of state of the art and case histories, in *Monitoring and Mitigation of Volcano Hazards*, edited by R. Scarpa and R. Tilling, pp. 99–147, Springer, Berlin.
Miller, A. D., R. C. Stewart, R. a. White, R. Luckett, B. J. Baptie, W. P. Aspinall, J. L. Latchman, L. L. Lynch, and B. Voight (1998), Seismicity associated with dome growth and collapse at the Soufriere Hills Volcano, Montserrat, *Geophys. Res. Lett.*, *25*, 3401–3404, doi:10.1029/98GL01778.
Moran, S. C., C. Newhall, and D. C. Roman (2011), Failed magmatic eruptions: Late-stage cessation of magma ascent, *Bull. Volcanol.*, *73*, 115–122.
MVO (2008), MVO OFR 08/02, *MVO Open File Rep. 08/02*, pp. 20–22.
Neuberg, J., and C. O'Gorman (2002), A model of the seismic wavefield in gas-charged magma: Application to Soufriere Hills Volcano, Montserrat, *Geol. Soc. London Mem.*, *21*, 603–609.
Neuberg, J., R. Luckett, B. Baptie, and K. Olsen (2000), Models of tremor and low-frequency earthquake swarms on Montserrat, *J. Volcanol. Geotherm. Res.*, *101*, 83–104.
Neuberg, J., H. Tuffen, L. Collier, D. Green, T. Powell, and D. Dingwell (2006), The trigger mechanism of low-frequency earthquakes on Montserrat, *J. Volcanol. Geotherm. Res.*, *153*, 37–50.
Nicholson, E. J., T. A. Mather, D. M. Pyle, H. M. Odbert, and T. Christopher (2013), Cyclical patterns in volcanic degassing revealed by SO2 flux timeseries analysis: An application to Soufrière Hills Volcano, Montserrat, *Earth Planet. Sci. Lett.*, *375*, 209–221.
Nishimura, T., M. Iguchi, H. Yakiwara, J. Oikawa, R. Kawaguchi, H. Aoyama, H. Nakamichi, Y. Ohta, and T. Tameguri (2013), Mechanism of small vulcanian eruptions at Suwanosejima volcano, Japan, as inferred from precursor inflations and tremor signals, *Bull. Volcanol.*, *75*(779), 1–12.
Ogburn, S. E., S. C. Loughlin, and E. S. Calder (2015), The association of lava dome growth with major explosive activity (VEI $\geq$ 4): DomeHaz, a global dataset, *Bull. Volcanol.*, *77*(40), 1–17.
Ottemöller, L. (2008), Seismic hybrid swarm precursory to a major lava dome collapse: 9–12 July 2003, Soufriere Hills Volcano, Montserrat, *J. Volcanol. Geotherm. Res.*, *177*, 903–910.
Paulatto, M., C. Annen, T. J. Henstock, E. Kiddle, T. A. Minshull, R. S. J. Sparks, and B. Voight (2012), Magma chamber properties from integrated seismic tomography and thermal modeling at Montserrat, *Geochem. Geophys. Geosyst.*, *13*, Q01014, doi:10.1029/2011GC003892.
Petersen, T. (2007), Swarms of repeating long-period earthquakes at Shishaldin Volcano, Alaska, 2001–2004, *J. Volcanol. Geotherm. Res.*, *166*, 177–192.
Plail, M., M. Edmonds, M. C. S. Humphreys, J. Barclay, and R. A. Herd (2014), Geochemical evidence for relict degassing pathways preserved in andesite, *Earth Planet. Sci. Lett.*, *386*, 21–33.
Power, J. A., S. D. Stihler, B. A. Chouet, M. M. Haney, and D. M. Ketner (2013), Seismic observations of Redoubt Volcano, Alaska - 1989–2010 and a conceptual model of the Redoubt magmatic system, *J. Volcanol. Geotherm. Res.*, *259*, 31–44.
Preece, K., R. Gertisser, J. Barclay, S. J. Charbonnier, J. C. Komorowski, and R. A. Herd (2016), Transitions between explosive and effusive phases during the cataclysmic 2010 eruption of Merapi volcano, Java, Indonesia, *Bull. Volcanol.*, *78*(54), 1–16.
Rodgers, M., D. C. Roman, H. Geirsson, P. LaFemina, A. Muñoz, C. Guzman, and V. Tenorio (2013), Seismicity accompanying the 1999 eruptive episode at Telica Volcano, Nicaragua, *J. Volcanol. Geotherm. Res.*, *265*, 39–51.
Rodgers, M., S. Rodgers, and D. C. Roman (2015a), Peakmatch: A java program for multiplet analysis of large seismic datasets, *Seismol. Res. Lett.*, *86*, 1208–1218.
Rodgers, M., D. C. Roman, H. Geirsson, P. LaFemina, S. R. McNutt, A. Muñoz, and V. Tenorio (2015b), Stable and unstable phases of elevated seismic activity at the persistently restless Telica Volcano, Nicaragua, *J. Volcanol. Geotherm. Res.*, *290*, 63–74.
Roman, D. C., and K. V. Cashman (2006), The origin of volcano-tectonic earthquake swarms, *Geology*, *34*, 457–460.
Roman, D. C., M. Rodgers, H. Geirsson, P. C. LaFemina, and V. Tenorio (2016), Assessing the likelihood and magnitude of volcanic explosions based on seismic quiescence, *Earth Planet. Sci. Lett.*, *450*, 20–28.
Rowe, C. A., C. H. Thurber, and R. A. White (2004), Dome growth behavior at Soufriere Hills Volcano, Montserrat, revealed by relocation of volcanic event swarms, 1995–1996, *J. Volcanol. Geotherm. Res.*, *134*, 199–221.
Rutherford, M. J., and J. D. Devine (2003), Magmatic conditions and magma ascent as indicated by hornblende phase equilibria and reactions in the 1995-2002 Soufrière Hills magma, *J. Petrol.*, *44*, 1433–1454.
Self, S., L. Wilson, and I. A. Nairn (1979), Vulcanian eruption mechanisms, *Nature*, *277*, 440–443.
Smith, P. (2013), *Volcano-Tectonic Seismicity of Soufriere Hills Volcano, Montserrat*, *Encycl. of Earthquake Eng.*, Springer, Berlin.
Sparks, R. S. J. (1997), Causes and consequences of pressurisation in lava dome eruptions, *Earth Planet. Sci. Lett.*, *150*, 177–189.
Sparks, R. S. J. (2003), Forecasting volcanic eruptions, *Earth Planet. Sci. Lett.*, *210*, 1–15.
Stix, J., R. C. Torres, L. Narváez M, G. P. Cortés J, J. A. Raigosa, D. Gómez M, and R. Castonguay (1997), A model of vulcanian eruptions at Galeras volcano, Colombia, *J. Volcanol. Geotherm. Res.*, *77*, 285–303.
Sturton, S., and J. Neuberg (2003), The effects of a decompression on seismic parameter profiles in a gas-charged magma, *J. Volcanol. Geotherm. Res.*, *128*, 187–199.
Sturton, S., and J. Neuberg (2006), The effects of conduit length and acoustic velocity on conduit resonance: Implications for low-frequency events, *J. Volcanol. Geotherm. Res.*, *151*, 319–339.
Surono, J. P., et al. (2012), The 2010 explosive eruption of Java's Merapi volcano—A "100-year" event, *J. Volcanol. Geotherm. Res.*, *241-242*, 121–135.
Swanson, S. E., M. T. Naney, H. R. Westrich, and J. C. Eichelberger (1989), Crystallization history of Obsidian Dome, Inyo Domes, California, *Bull. Volcanol.*, *51*, 161–176.
Tait, S., C. Jaupart, and S. Vergniolle (1989), Pressure, gas content and eruption periodicity of a shallow, crystallizing magma chamber, *Earth Planet. Sci. Lett.*, *92*, 107–123.
Thelen, W., S. Malone, and M. West (2011), Multiplets: Their behavior and utility at dacitic and andesitic volcanic centers, *J. Geophys. Res.*, *116*, B08210, doi:10.1029/2010JB007924.
Thomas, M. E., and J. Neuberg (2012), What makes a volcano tick—A first explanation of deep multiple seismic sources in ascending magma, *Geology*, *40*, 351–354.

Tripoli, B. A., B. Cordonnier, A. Zappone, and P. Ulmer (2016), Effects of crystallization and bubble nucleation on the seismic properties of magmas, *Geochem. Geophys. Geosyst.*, *17*, 602–615, doi:10.1002/2015GC006123.

Tuffen, H., and D. Dingwell (2005), Fault textures in volcanic conduits: Evidence for seismic trigger mechanisms during silicic eruptions, *Bull. Volcanol.*, *67*, 370–387.

Varley, N. R., R. Arámbula-Mendoza, G. Reyes-Dávila, J. Stevenson, and R. Harwood (2010), Long-period seismicity during magma movement at Volcán de Colima, *Bull. Volcanol.*, *72*, 1093–1107.

Voight, B. (1988), A method for prediction of volcanic eruptions, *Nature*, *332*, 125–130.

Wadge, G., G. S. Mattioli, and R. A. Herd (2006), Ground deformation at Soufrière Hills Volcano, Montserrat, during 1998–2000 measured by radar interferometry and GPS, *J. Volcanol. Geotherm. Res.*, *152*, 157–173.

Wadge, G., B. Voight, R. S. J. Sparks, P. D. Cole, S. C. Loughlin, and R. E. A. Robertson (2014), An overview of the eruption of Soufriere Hills Volcano, Montserrat from 2000 to 2010, *Geol. Soc. London Mem.*, *39*, 1–40.

Watt, S. F. L., T. A. Mather, and D. M. Pyle (2007), Vulcanian explosion cycles: Patterns and predictability, *Geology*, *35*, 839–842.

West, M. E. (2013), Recent eruptions at Bezymianny volcano-a seismological comparison, *J. Volcanol. Geotherm. Res.*, *263*, 42–57.

White, R. A., A. D. Miller, L. Lynch, and J. Power (1998), Observations of hybrid seismic events at Soufriere Hills volcano, Montserrat: July 1995 to September 1996, *Geophys. Res. Lett.*, *25*, 3657–3660, doi:10.1029/98GL02427.

Young, N. K., and J. Gottsmann (2015), Shallow crustal mechanics from volumetric strain data: Insights from Soufriere Hills Volcano, Montserrat, *J. Geophys. Res. Solid Earth*, *120*, 1559–1571, doi:10.1002/2014JB011551.